

*Invited Paper*

## Application Advancement of Continuous-wave THz technology

Zhuangzhuang Fan, and Xinke Wang \*

Beijing Key Laboratory of Metamaterials and Devices, Department of Physics, Capital Normal University, Beijing  
100048, China

\* Email: wxk82721@cnu.edu.cn

(Received March 2025)

**Abstract:** Terahertz (THz,  $1\text{ THz}=10^{12}\text{ Hz}$ ) technology has been widely applied in multiple industrial fields based on characteristics of the THz radiation, including low photon energy, high transmission to nonpolar substances, broadband spectrum, and low scattering. Comparing to traditional optical methods, unique advantages of THz technology have been gradually recognized, including non-destructiveness, high resolution, high penetration to non-metallic materials, and high sensitivity. Comparing to a THz pulse system, continuous-wave THz (CW-THz) technology has a specific frequency, high stability, and simple system configuration. This paper partly reviewed application advancements of CW-THz technology in concealed object detection, non-destructive testing, medical imaging, and communications. The sources and detectors of CW-THz were briefly introduced. In addition, current technical challenges of CW-THz systems were also discussed. It could be envisioned that CW-THz technology was further commercialized in wider application fields through technological innovation, equipment optimization, and cost control. It would bring technical revolutions to industry, medicine, communications, and astronomical observation.

**Keywords:** Terahertz, Continuous-wave, Concealed Object Detection, Non-destructive Testing, Medical imaging, Communications.

**Doi:**

### 1. Introduction

Terahertz radiation ( $1\text{ THz}=10^{12}\text{ Hz}$ ) is an electromagnetic wave located between microwave and infrared radiation. Its frequency range is located between  $0.1\text{ THz}$  and  $10\text{ THz}$ , namely a  $30\text{ }\mu\text{m}\sim 3\text{ mm}$  wavelength range. Because of its location in the electromagnetic spectrum, the THz radiation possesses some characteristics of microwave and infrared radiation. Meanwhile, the THz radiation also has its unique physical properties and application potentials [1]. The THz radiation has characteristics of low photon energy, strong transmission to nonpolar substances, broadband spectrum, and low scattering. The THz radiation has a low photon energy (several  $\text{meV}$ ), which is much lower than ionizing radiation (such as X-rays or gamma rays). Therefore, it belongs to non-

ionizing radiation and had little damage to biological tissues. The THz radiation could penetrate various non-polar materials (such as paper, cloth, plastics). It is strongly reflected or absorbed by metallic materials or biological tissues. Many molecules has characteristic absorption peaks in the THz frequency band, especially organic molecules. These substances could be easily identified by THz spectroscopy. The THz wave has weaker scattering effects compared to optical bands so that it was suitable for imaging or communication.

Continuous-wave THz (CW-THz) generally refers to a continuous THz signal with a stronger power in a narrow bandwidth. Comparing to a THz pulse system, CW-THz technology has a specific frequency, high stability, and simple system configuration. Based on these advantages, CW-THz technology has shown powerful application potentials in many industrial fields. In this paper, the recent application advancements of CW-THz were partially reviewed, mainly including concealed object detection, non-destructive testing, medical diagnosis, and THz communications.

## 2. CW-THz Sources and Detectors

### A. CW-THz Sources

The generation of the CW-THz radiation depends on different physical mechanisms, including electronic, optical, and hybrid technology. The methods have unique advantages, which were adopted based on different application requirements (such as frequency range, power, coherence, etc.). The methods are briefly introduced in the following.

#### 1) Frequency multiplication

Frequency multiplication technology is a matured method for generating CW-THz radiation [2], especially for the high-precision CW-THz generation and the frequency control. In this method, a nonlinear device is used to multiply the frequency of a microwave or millimeter wave so that a desired THz frequency could be approached. In the device, a sinusoidal signal  $f_0$  is input and its high harmonics  $nf_0$  is generated due to the nonlinear response of the device. The harmonic frequency could be located on the THz frequency range if  $n$  is high enough. Generally, frequency multipliers could be  $n=3, 4, 6$ , even higher based on the target frequency and frequency multiplier design. The core of the frequency multiplier is nonlinear elements, such as a Schottky diode or nonlinear materials. Among them, a Schottky diode is one of the most commonly used frequency

multiplier devices. The frequency multiplication is achieved by using its nonlinear Volt-Ampere properties. In the frequency multiplication system, a frequency chain is formed by multi-stage frequency multiplication and high harmonics is output [3]. A typical frequency chain consists of a microwave source (such as a microwave oscillator) that generate a baseband signal, a power amplifier that amplify the signal to compensate the energy loss, a frequency multiplication cascade structure that gradually increase the frequency, and a filter that filter out unnecessary harmonics and extracts the target frequency. By using the method, the frequency of the output signal could approach from 0.1 THz to several THz. The output power of the THz radiation is generally between  $\mu W$  and  $mW$ . The frequency multiplication process is usually very stable based on the stability of the fundamental frequency source. Meanwhile, the output power gradually decrease with increasing the frequency multiplication. In addition, the nonlinear conversion efficiency of the frequency multiplication process is lower, so a high-power fundamental frequency signal is required. Nevertheless, the frequency multiplication technology is based on the stability of the fundamental frequency source and the frequency accuracy could reach a precision of the sub-hertz level. The manufacturing cost of a Schottky diode is relatively low. Besides, the frequency multiplication system could be integrated with other microwave or millimeter sources, which could be easily used in portable instruments. Therefore, frequency multiplication technology has good practicality, which is usually used in high-precision terahertz spectroscopy, communications, and imaging.

## 2) Difference frequency generation

Similar to frequency multiplication technology, difference frequency technology is also based on nonlinear optical effects [4]. When two laser beams  $f_1$  and  $f_2$  (usually visible light or near-infrared radiation) with different frequencies are coupled into a nonlinear crystal, they interact with each other to generate a difference frequency signal. The difference frequency is located on the THz band. The difference frequency signal is written as  $f_{\text{THz}} = |f_1 - f_2|$ . The frequency of the generated CW-THz wave could be adjusted by selecting appropriate incident lasers and nonlinear elements [5]. The frequency of the CW-THz wave could be varied from 0.1 THz to several THz. Meanwhile, a high frequency stability of the CW-THz wave could be guaranteed when high-stability continuous wave lasers were used as sources. The power and coherence of the CW-THz source are also higher in the technique. The difference frequency technology has a good application potential in high-precision THz spectroscopy.

## 3) Quantum cascade laser

Quantum cascade lasers (QCL) are based on semiconductor heterostructures [6], which formed a multi-layer periodic superposition structure through quantum wells and quantum barriers. In this structure, electrons undergo controlled tunneling and energy level transition processes in the quantum wells, which emit photons of a specific frequency. The output wavelength of QCL is completely determined by the energy band design, which could approach the THz frequency band. QCLs are usually composed of quantum well structures based on III-V semiconductors (such as GaAs/AlGaAs or InGaAs/InAlAs). In order to operate in the THz band, the electron mobility and bandgap characteristics of the semiconductors are crucial. The active region of a QCL consist of multiple periods of quantum well structures. Each period contain three crucial energy levels, namely an upper energy level  $E_3$ , an intermediate energy level  $E_2$ , and a ground state  $E_1$ . Electrons transferred from the level  $E_3$  to the level  $E_2$  by radiative transition. Then, the electrons transfer to the ground state  $E_1$  by non-radiative tunneling. Finally, the electrons are re-excited to the upper energy level  $E_3$  through the injection region and a new cycle is started. The frequency of the photons is determined by the energy difference between the upper and middle energy levels  $\Delta E = E_3 - E_2$  and the frequency could be expressed as  $f_{\text{THz}} = \Delta E/h$ , where  $h$  was the Planck constant. The frequency range of quantum cascade lasers is usually from 1 THz to 5 THz. At the same time, the output frequency could be flexibly adjusted by changing widths, thicknesses, and materials of quantum wells. By using the technique, the CW-THz source has a high-power output, high frequency accuracy, good coherence, and good integration [7]. Comparing with other CW-THz sources (such as photoconductive antennas or frequency multiplication), QCLs could provide an output power of tens of  $mW$ . In addition, QCLs have extremely high frequency stability and repeatability. The THz radiation generated by QCLs has a very narrow spectral line width (usually in the MHz range), which is suitable for high-precision THz spectroscopy and interferometry. Because QCLs are based on semiconductor technology, it could be easily integrated with other optoelectronic devices, which make it suitable for portable devices.

## B. CW-THz Detectors

Various methods are employed to detect CW-THz signals. The techniques could be divided into three categories based on different mechanisms, including thermal effect detection, electromagnetic field detection, and photonic property detection [8]. In addition, microwave resonant cavities and high-speed electronic detectors based on microwave technology could also be used for the THz detection. In this field, the most common methods mainly contain thermoelectric detectors, photoconductive detectors, and frequency mixing detectors.

### 1) Thermoelectric detectors

The core principle of thermoelectric detectors is that the THz radiation was absorbed by materials, which is converted into heat. The accumulation of heat cause the temperature change inside the device. Then, the temperature change is converted into an electrical signal [9]. Therefore, the sensitivity of the device is related to the absorption coefficient of materials, thermal conductivity characteristics, and electrical characteristics of the sensor element. The response range of thermoelectric detectors could cover a wide frequency range from microwaves to far infrared, which makes them ideal for the THz detection. The detection capability of thermoelectric detectors is good for CW-THz sources with lower powers, which could work in the power ranging from  $nW$  to  $\mu W$ . It makes the detectors suitable for basic researches and low-power signal detection under laboratory conditions. However, the response time of thermoelectric detectors is usually the order of millisecond due to the slow heat transfer and temperature rise processes. It limits applications of the detectors in high-dynamic or fast-modulated THz signals.

### 2) Photoconductive detectors

The basic principle of photoconductive detectors is the photoinduced current excited by a pump laser and THz field on a photoconductive antenna. Electron-hole pairs between electrodes are excited when pump lasers are used to irradiate semiconductors (such as GaAs). Then, the THz electric field is exerted on the photoconductive antenna and the photoinduced current is formed between electrodes. The intensity and frequency of the photoinduced current reflect the characteristics of the THz wave. The photoinduced current is measured by an external circuit and the CW-THz signal is extracted by analyzing the current. The sensitivity of photoconductive detectors is very high to the THz radiation, which could response to a THz signal with  $nW$  power [10]. At the same time, the noise level of the devices is also lower due to their inherent narrowband filtering effect. Based on material properties and designs of photoconductive antennas, a sub-hertz frequency resolution could be achieved, which is suitable for CW-THz spectroscopy. In addition, the frequency response of photoconductive detectors could be adjusted from 0.1 THz to 3 THz by controlling the antenna design (such as dipole antennas or logarithmic periodic antennas). Besides, photoconductive detectors have compact physical structures, which could be integrated with other optical systems. Therefore, photoconductive detectors have been widely applied in CW-THz imaging and spectroscopy.

### 3) Frequency mixing detectors

The core of frequency mixing detectors is to mix a THz signal and a stable local oscillator signal in a nonlinear element. Then, a difference frequency (or beat frequency) signal is extracted and analyzed [11]. In the mixer, a nonlinear coupling between the THz signal ( $f_{\text{THz}}$ ) and local oscillator signal ( $f_{\text{LO}}$ ) are formed to generate a series of harmonic frequency components which contained a difference frequency signal ( $f_{\text{IF}} = |f_{\text{THz}} - f_{\text{LO}}|$ ). The difference frequency signal generally is located on the radio frequency range, which could be amplified and analyzed by external circuits. The amplitude, phase, and frequency of the difference frequency signal contain the information of the THz signal. For instance, the nonlinear characteristics of Schottky diodes are utilized to mix a THz signal and local oscillator signal. The measurement of a THz signal could be quickly completed at room temperature. However, the sensitivity of the method is relatively lower, which is only suitable for the high-power THz sources. Based on the electron heating effect of superconductor mixers, the devices have sensitive responses to weak THz signals and the operating frequency could reach several THz. However, the devices need work in a low-temperature environment and their systems were complex.

### 3. Applications of CW-THz

Based on unique inspection capabilities, CW-THz technology has been applied in multiple industrial fields. Applications of CW-THz technology are partly reviewed in concealed object detection, non-destructive testing, medical imaging, and communications in this section.

#### A. Concealed Object Detection

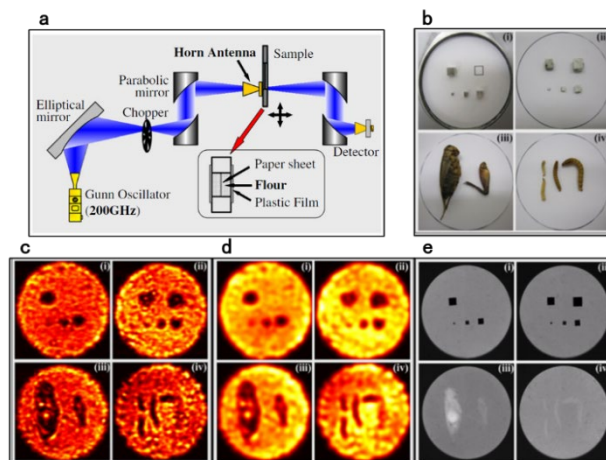


Fig. 1 (a) Transmission CW-THz imaging system operating at 0.2 THz; (b) Optical images of foreign matters in flour, including metal cubes, cubic stones, grasshoppers, and mealworms; (c), (d) CW-THz images of foreign matters in flour. (c) presented original images and (d) presented optimized images after average filtering. (e) X-ray images of the samples [12].

Because the high transmittance of non-polar materials and the high reflectivity of metallic materials to the THz radiation, CW-THz technology has become an important inspection method in concealed object detection. With the development of THz sources, detectors, and systems, the application has become more and more mature. Many illegal and dangerous substance could be readily identified by the technique, such as explosives and drugs. In 2012, a transmission-type CW-THz imaging system was employed by G.-J. Kim *et al.* to examine organic substances inside food and the feasibility of CW-THz imaging was demonstrated [12]. Comparing to X-rays, the THz system showed relatively higher sensitivities for organic samples. The CW-THz source was a frequency-multiplied Gunn oscillator operating at 0.2 THz, as shown in Fig. 1(a). Its output power was beyond 10 mW. The THz wave radiated by the Gunn oscillator was focused by an elliptical mirror and a mechanical chopper with 1 kHz was used to control the output of the THz beam. Then, the THz beam was collimated and focused by four parabolic mirrors in sequence. A zero-bias GaAs Schottky diode with a sensitivity of 250 V/W was employed as a detector to detect the THz signal and a lock-in amplifier was used to extract the THz signal. In this work, four common foreign matters were selected as the measured objects, including metal cubes, cubic stones, grasshoppers, and mealworms. Figure 1(b) presented the optical images of the foreign bodies. The sizes of the metal cubes were adjusted from  $1\times 1\times 1\text{ mm}^3$  to  $4\times 4\times 4\text{ mm}^3$ . The sizes of the cubic stones were varied from  $1\times 1\times 1\text{ mm}^3$  to  $5\times 5\times 5\text{ mm}^3$ . The maximum thickness of the grasshoppers approximately reached 7 mm. The diameters of the mealworms were in range from 1 mm to 3 mm. Four type of foreign bodies were covered by flour and their CW-THz images were acquired, as shown Figs. 1(c) and (d). Fig. 1(c) presented the original THz images of the samples. The unevenness of the images was caused by the density difference of flour. Average filtering was fulfilled to optimize the THz images and the noise effect was reduced, as shown in Fig. 1(d). The foreign bodies in the filter images could be more readily identified from the filtered images. For comparison, the samples were measured by X-ray imaging. Figure 1(e) presented the measurement results. Obviously, the sharpness of metal cubes and cubic stones in X-ray images was better than THz images. However, THz images of biological tissues (grasshoppers and mealworms) exhibited more clear contrast because the THz wave could strongly interact with the water content in biological tissues. The property ensured that THz imaging could become an important complementary technology with X-ray and optical imaging.

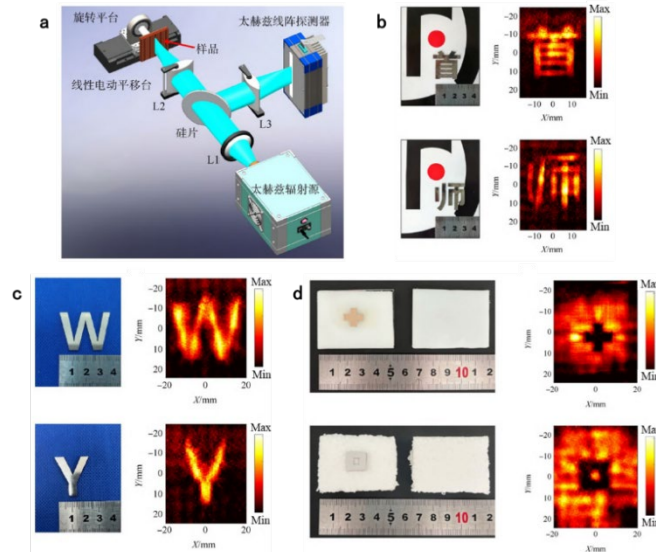


Fig. 2 (a) Reflective CW-THz line scan imaging system; (b), (c) Imaging of metallic samples hidden in envelopes and textiles; (d) Non-invasive detection of foreign objects in polyethylene and foam plastic boards [13].

In 2024, a reflective CW-THz line scan imaging system with a THz linear array detector and a  $0.3\text{ THz}$  source was built by Y. C. Wang *et al.* [13], as shown in Fig. 2(a). Through twice scan measurements and image linear superposition, an CW-THz image reflected by a sample could be accurately measured with a resolution of  $2\text{ mm}$ , measurement region of  $40\text{ mm}\times 40\text{ mm}$ , and measurement time of less than  $3\text{ min}$ . This system was successfully used to identify metallic samples hidden in envelopes and textiles. In addition, foreign objects embedded in polyethylene boards and foam plastic boards were also accurately located. As shown in Fig. 2(b), two metallic Chinese characters “首” and “师” with a  $4\text{ mm}$  line width and a  $2\text{ mm}$  thickness were fabricated. Their sizes were  $29\text{ mm}\times 30\text{ mm}$  and  $31\text{ mm}\times 28\text{ mm}$ , respectively. The characters were hidden in an envelope, which could be not observed from the appearance. The samples were measured using the CW-THz imaging system and each measurement only took about  $3\text{ min}$ . From experimental results, it could be seen that the distributions of the characters could be clearly identified although the signal-to-noise ratio of imaging was affected by the envelope to a certain extent. Using the same method, two metallic letters “W” and “Y” wrapped in non-woven fabrics were also measured, as shown in Fig. 2(c). It could be seen that the features of the letters could still be accurately identified from the THz images under wrapping of non-woven fabrics. These results sufficiently verified the detection capability of this imaging system for hidden objects. In addition, THz detection equipment was also usually used for non-invasive flaw detection of internal defects in various packaging or building materials due to high transmittance of the THz radiation to non-polar substances. In this work, the testing capability of the system to pre-embedded foreign bodies in polyethylene and foam plastic boards was also demonstrated. A cross-shaped cardboard was fixed

between two polyethylene boards to simulate foreign bodies inside the polyethylene board and a square-shaped cardboard was fixed between two foam plastic boards to simulate foreign bodies inside the foam plastic board, as shown in Fig. 2(d). The sizes of the foreign bodies were  $13\text{ mm}\times 13\text{ mm}$  and  $14\text{ mm}\times 13\text{ mm}$ , respectively. Their line widths and thicknesses were  $5\text{ mm}$  and  $0.5\text{ mm}$ . The two samples were measured using the imaging system. In order to enhance the image quality, a metal plate was fixed behind the sample to increase the reflectivity of the THz signal. The detection time for each sample was also about  $3\text{ min}$ . From experimental result, it could be seen that the intensities of reflective THz signals were significantly weakened on the regions of foreign objects due to strong scattering and absorption effects of the objects to THz waves. Therefore, the distributions of the objects could be exactly exhibited from THz images. This work verified that this system had a good detection capability for foreign objects inside packaging and building materials.

There are still some recent studies in this field. In 2012, a real-time active CW-THz imaging system was built by A. C. Torrezan *et al.* with a  $0.46\text{ THz}$  cyclotron capable of generating  $16\text{ W}$  CW-THz waves and a pyroelectric array camera with  $124\times 124$  pixels [14]. In this work, real-time video of paper envelopes containing metal samples was separately taken in transmission and reflection measurement modes, which demonstrated that the real-time CW-THz imaging system could inspect visually opaque materials. In 2014, a real-time CW-THz line scan imaging system based on a  $1\times 240$  InGaAs Schottky Barrier diode (SBD) array detector was built by S. -P. Han *et al.* [15], which possessed a scan speed of  $25\text{ cm/s}$ , a scan line length of  $12\text{ cm}$ , and a pixel size of  $0.5\times 0.5\text{ mm}^2$ . A paper clip hidden under a cookie was successfully detected by the system with a spatial resolution of  $1\text{ mm}$ . In 2016, a circularly polarized frequency-modulated continuous-wave (FMCW) radar operating near  $210\text{-}270\text{ GHz}$  was proposed by J. Grzyb *et al.* [16]. The radar included a highly integrated RF transceiver module, an internally developed frequency linear FM generator, and a data acquisition chain. A cardboard box containing a drug blister package was measured by the system. The peaks associated with the reflection of the cardboard box, plastic cavity and aluminum foil seal were clearly separated and missing tablets in the drug package was successfully identified. In 2019, a CW-THz CT imaging system using Bessel beams generated by conical lenses was reported by D. Y. Wang *et al.* [17]. In this work, the system was used to obtain different two-dimensional cross-sectional images of the internal structure of the blocked plastic pipe. In 2024, a THz perspective ranging technology based on linear frequency modulated continuous wave was proposed by Z. Y. Zhou *et al.*, which realized the measurement of thicknesses of various materials and the dielectric constants of multi-layer dielectric materials under a non-contact mode [18].

## B. Non-destructive Testing

The application of CW-THz technology in non-destructive testing (NDT) is gradually developed as an important technical means. Comparing to traditional detection methods (such as X-rays and ultrasonic waves), CW-THz technology has non-destructiveness, high resolution, high penetration to non-metallic materials, high sensitivity, and other advantages. In recent years, application progress of CW-THz was very significant in non-destructive testing, particularly in material testing, structural health monitoring, defect detection, and quality control. In 2019, a scan imaging system was built by B. Wang using a 0.3 THz radiation source and a linear array detector [19]. The output power of the radiation source was about 14 mW. The pixel size of the detector was 0.5 mm × 0.5 mm and its number of pixels was 256×1 pixels. The acquisition speed of the detector could reach 100 frame/s. The schematic diagram and photo of the imaging system are shown in Figs. 3(a) and 3(b). The 0.3 THz beam was transmitted to free space through a horn antenna. The THz beam was focused in one dimension by a metallic off-axis concave reflector to form a focal line, which was focused on the detector for sample scanning. By successively varied the sample position, the sample was entirely scanned by the THz focal line and the THz image of the sample was built. During measurement, the sample was always close to the detector as possible to reduce the diffraction influence and acquire a higher resolution. Because the system needed not a two-dimensional scan operation and the THz linear array detector had a fast response speed, the measurement time was greatly shortened. Fig. 3(c) showed the distribution of the THz focal line which was measured on the focal plane of the concave reflector. It could be seen that the THz wave was focused into a narrow line. The uneven distribution of the focal line was caused by the unevenness of the THz spot and the response discrepancy of the detector. An intensity curve was extracted along the x-axis direction, which was marked by the white dashed line in Fig. 3(c). Figure 3(d) presents the intensity profile curve which had a half maximum full width (HMFV) of 3.5 mm. In addition, some weak diffraction fringes were observed on the left side of the main focal line due to the diffraction influence. Fortunately, the intensities of these side lobes were too weak to significantly affect the imaging effect. To test the resolution of the system, a steel resolution plate was measured, as shown in Fig. 3(e). The THz image of the resolution plate was acquired and the morphology of the sample was clearly observed, as shown in Fig. 3(f). The gaps above 1.5 mm could be distinctly resolved. The imaging system was used to measure embedded defects inside a polyethylene board. The polyethylene board with a 25 mm thickness was selected as the sample and four scratches were processed on the back of the sample, as shown in Fig. 3(g). The interval between adjacent scratches was about 20 mm. The length and width of each scratch were 40 mm and 0.5 mm. Their depths were 5, 5, 2, and 1 mm, respectively. In addition, a polyethylene board

with internal hole defects was prepared as another sample, as shown in Fig. 3(j). Five circular hole defects were fabricated inside the sample. The interval between adjacent defects was about 15 mm. The diameters of the five holes were 0.2, 0.5, 1, 1.5, and 2 mm from left to right. The sample was scanned by the imaging system with the imaging area of 100 mm×100 mm and the scan step of 1 mm. The measurement time was only about 1 min. Figures 3(h) and 3(k) showed THz images of the samples, respectively. Almost all scratch and hole defects could be clearly identified. The intensity curves were extracted along red dashed lines in Figs. 3(h) and 3(k). Figures 3(i) and 3(l) showed the intensity curves of the scratch and hole defects. Although the imaging resolution was about 1.5 mm, the defects with a 0.5 mm width could still be identified. However, the hole defect with a 0.2 mm diameter could be not located because the defect size was much smaller than the system resolution limit. The work demonstrated that CW-THz imaging system could successfully identify different type of defects, which was valuable for industrial non-destructive testing. In addition, the system adopted a linear scan measurement mode to achieve fast acquiring of a THz image and greatly shortened the measurement time.

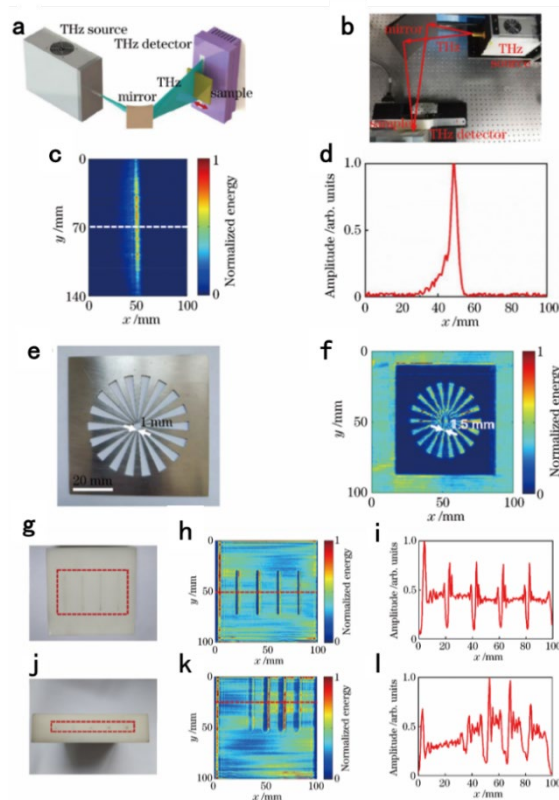


Fig. 3 0.3 THz linear array scan imaging system and measurement results. (a) System schematic diagram; (b) Photo of the system; (c) Distribution of the THz focal line; (d) Intensity curve extracted along the white dashed line from Fig. 3(c); (e) Photo of steel resolution plate; (f) THz image of resolution plate; (g)-(l) THz imaging of internal scratch and hole defects of polyethylene boards [19].

In 2022, Jue Hu *et al.* proposed an autonomous dynamic line-scan CW-THz non-destructive inspection system [20]. The system integrated CW-THz and long-wave infrared radiation (LWIR) thermography techniques for testing of cultural relics. The line-scan CW-THz imaging system consisted of a linear array detector, a CW-THz emitter, and an x-y scan stage. The spectral response range of the detector could approach  $0.7\text{ THz}$  and its sample rate was  $8.2\text{ fps}$ . The imaging area was about  $6\times 384\text{ mm}$ . Fig. 4(a) shows the schematic diagram and experimental configuration of the system. Figure 4(b) shows the photo of a mosaic sample constituted by different type of wood used for nondestructive testing. There were three manufactured defects inside the sample. In the left side, a circular flat-bottomed groove was punched on the upper layer of the sample. In the middle, a circular hole that penetrated the sample was presented. In the right side, a circular flat-bottomed groove was punched in the bottom surface of the sample. Figure 4(c) shows the LWIR imaging result of the sample. From results, the defects A and B near the surface were easily detected. However, the defect C could not be effectively identified because it was near the bottom surface of the sample. By combing the CW-THz and LWIR imaging results, the final measurement result of the sample was given by utilizing an enhanced unsupervised deep feature fusion (UDFF) algorithm, as shown in Fig. 4(d). In that case, three artificial holes were clearly recognized. Hidden defects in the wood structure could be detected by CW-THz imaging and surface and sub-surface defects could be measured by LWIR imaging. The high-dimensional features of the sample were effectively extracted by the UDFD algorithm through a deep encoder structure with dense connections and residual modules. It ensured that the method was highly robust to background noise and effectively fused the detailed information of the input data. This work showed that the method could effectively and automatically detect defects on workpieces.

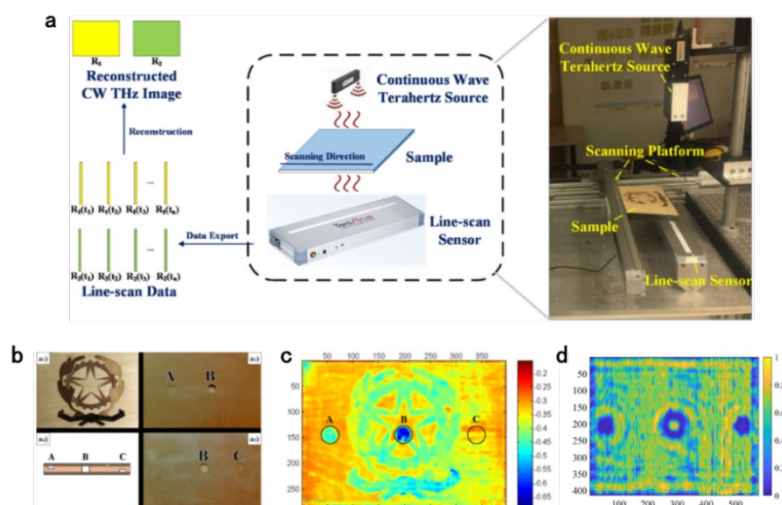


Fig. 4 (a) Dynamic line scan CW-THz imaging system; (b) Mosaic sample; (c) LWIR imaging result of the mosaic sample; (d) CW-THz imaging result using UDFD algorithm [20].

In 2023, B. N. Kumar *et al.* combined dynamic depth focusing (DDF) technology with CW-THz imaging to evaluate the qualities of low-temperature foams [21]. In this work, two near-infrared radiation distributed feedback (DFB) lasers were mixed in a 50/50 combiner whose output was fed to a THz transmitter. The output frequency of the THz transmitter could be adjusted from 0.1 THz to 0.8 THz. In addition, the system still contained polymethylpentene (TPX) lenses and a THz receiver, as shown in Fig. 5(a). Here, a multi-layer coated cryogenic foam sample containing artificial defects were measured. The foam sample had a size of 100 mm×100 mm. Two defects with the sizes of 20 mm×20 mm×2 mm and 30 mm×30 mm×3 mm were manufactured on the back side of the sample. The foam was fixed on an aluminum plate using a cryogenic-compatible adhesive. The sample was fixed on a two-dimensional stage and imaged using the system. Normalized amplitude images at 0.1 THz, 0.15 THz, 0.2 THz, 0.3 THz, and 0.35 THz as well as the final synthetic result were obtained, as shown in Fig. 5(b). After dynamically adjusting the focus in the foam sample, metal-foam debonding areas exhibited higher contrast than surrounding healthy areas at all operating frequencies. It could be observed that some random local high-intensity areas appeared in THz images with different frequency components. Meanwhile, high-frequency images showed a higher resolution for detecting metal-foam debonding. Overall, the random noise was weakened and the defect areas in the sample were highlighted by compositing images with multi-frequencies. In addition, it should be pointed out that the image sharpness of the defects was influenced by the scattering effect of the porous foam to THz waves. The results showed that the THz dynamic deep focusing non-destructive testing technique could be used to evaluate the structural integrity of metal-foam bonding in multi-layer coated cryogenic foam insulation layers, which were very valuable for testing aerospace cryogenic storage tanks.

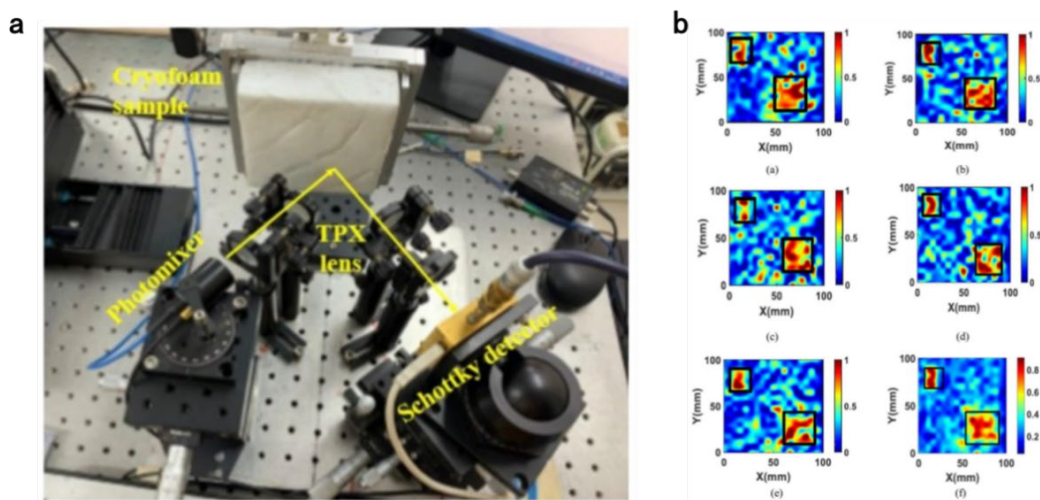


Fig. 5 (a) Reflection-mode CW-THz imaging system for measuring multilayer coated foam samples; (b) CW-THz images of multilayer coated foam samples at 0.1, 0.15, 0.2, 0.3, 0.35 THz and the final synthetic result [21].

There are still some recent studies in this field. In 2018, reflective frequency-modulated CW-THz system was used by Y. Zhou *et al.* to test multi-layer heat shields made of special materials [22]. The image data was processed by continuous wavelet transform with different basis functions and the defect regions could be accurately identified. In 2021, H. -S. Kim *et al.* achieved a non-destructive evaluation of cement hydration using a CW-THz system [23]. In this work, the relationship between the hydration degree of cement and the transmitted/reflected THz waves was studied. A new hydration prediction model was also proposed by combining the chemical composition and microstructure of cement measured by Fourier transform infrared spectroscopy (FT-IR) and scanning electron microscopy (SEM). In 2022, a THz three-dimensional imaging system for non-destructive testing of PE pipes was designed by J. Xu *et al.* [24]. The system was based on frequently modulated continuous wave (FMCW) technology with a CW-THz source bandwidth of 0.225-0.330 THz and an output power of more than 5 mW, which ensured a sub-millimeter spatial resolution in three dimensions. The system was used for 3D scanning of PE pipes in a laboratory environment and the results showed that the system could achieve non-destructive testing and 3D imaging of different defects in PE pipes.

### C. Medical Imaging

Recently, applications of CW-THz technology in medical imaging have been significantly advanced due to its sensitive responses to normal and diseased tissues. In particular, application potentials of CW-THz technology have been gradually recognized in cancer detection, skin disease diagnosis, and tissue imaging. With the development of THz sources and detectors, CW-THz imaging systems are gradually moved towards clinical medical applications. In 2018, CW-THz technology and computed tomography (CT) were combined by B. Li *et al.* to measure the internal structure of dry chicken ulna [25]. The schematic diagram of the THz-CT imaging system was shown in Fig. 6(a). The imaging system consisted of a backward wave oscillator (BWO) and a Golay detector. After measurement, a filtered back projection algorithm was used to reconstruct a two-dimensional cross-sectional image of the sample. The chicken ulna was composed of the diaphysis and proximal epiphysis. The proximal epiphysis mainly included dense grid-like spongy bones. From the two-dimensional cross-section, it was observed that the proximal epiphysis consisted of periosteum, compact bone, spongy bone, and bone marrow, as shown in Fig. 6(b). Through imaging, two-dimensional cross-sectional images at five locations of the sample were obtained. Irregular light and dark regions appeared in the central part of the THz image. The reason was that the liquid bone marrow and spongy bone marrow in the bone marrow cavity had different absorption coefficients to the THz radiation. The reconstructed cross-sectional image and the

absorption coefficient variation from position I to position V showed that, the closer to the proximal epiphysis, the smaller the bone marrow cavity became. The experiment showed that CW-THz CT imaging technology could be applied to 3D imaging of biological hard tissues such as teeth and bones. Because of the low water content of hard tissues, the sample's absorption effect to THz waves was smaller, which allowed that the clear structural information of dehydrated tissues was obtained through CW-THz CT imaging. Rich information of bone tissues could be readily acquired from THz images, including the absorption, refractive index, and density distribution.

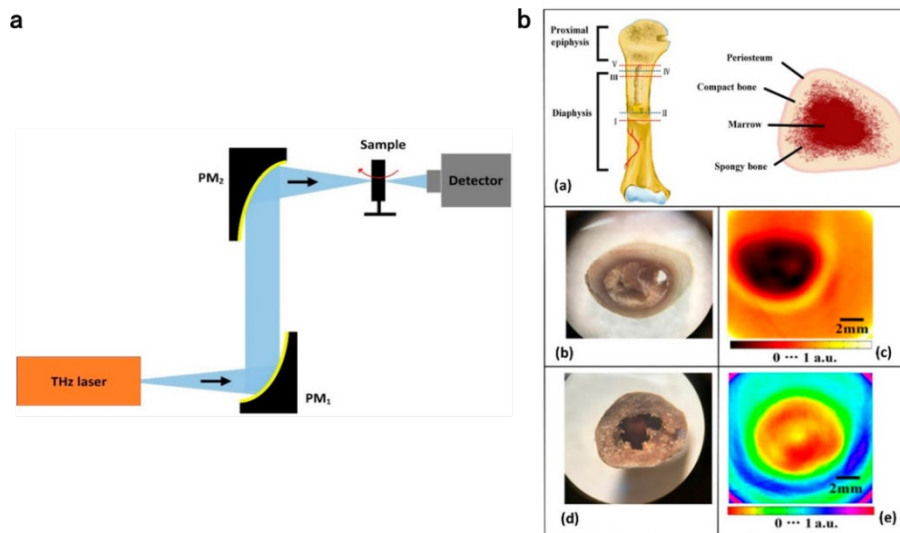


Fig. 6 (a) Schematic diagram of the THz computed tomography (THz-CT) imaging system; (b) Photos and THz images of dry chicken ulna [25].

In 2022, the influence of the THz polarization on the imaging performance of biological samples was studied by L. M. Wu *et al.* Fig. 7(a) shows the setup of the CW-THz reflection imaging system [26]. The study used a tunable optically pumped CW-THz gas laser with an operating frequency of 2.52 THz and a maximum output power of 150 mW. To reduce the influence of laser power fluctuations on imaging results, a wire grid beam splitter was used to separate the THz wave into two beams, including the sample light and the reference light. The reference light was directly received by a Golay detector. The sample light was reflected and focused by a gold-coated mirror and an off-axis parabolic mirror. The THz wave was focused onto the upper surface of the reflection window. The sample was placed on the objective stage, which was in close contact with the bottom of the reflection window. A two-dimensional stage was used to successively vary the position of the sample with a scan speed of approximately 10 pixels/s and a scan step of 200  $\mu\text{m}$ . Then, the THz image of the sample was built. The signal light carrying the sample information was received by another Golay detector. Figures 7(b)A and 7(b)B shows optical and THz images of a pork tissue

with an area of  $10 \times 10 \text{ mm}^2$  with a p-polarization. The refractive indices of lean and fat tissues were 1.85 and 1.6 at  $2.52 \text{ THz}$ , respectively. Considering the evaporation of water between two experiments, a new pork tissue with an area of  $10 \times 10 \text{ mm}^2$  was measured using s-polarized THz waves and the THz image with a s-polarization was acquired, as shown in Figs. 7(b)C and 7(b)D. These THz images were synthetically analyzed based on relative reflectivities. Lean and fat tissues could be clearly distinguished under both p- and s-polarization. The average reflectivities and standard deviations of lean tissues with p- and s-polarization were  $52\% \pm 2\%$  and  $70\% \pm 5\%$ , respectively. The results showed that the image contrast could be enhanced with a p-polarization. Therefore, the polarization of the THz beam should be carefully selected according to characteristics of a sample for obtaining the best sample information and image contrast. At the same time, the appropriate reflection window should be also properly chosen based on the refractive index of a sample. The image contrast could be improved by a reflection window with constructive interference. By further improving the resolution and imaging speed, the identification of biological tissues through in situ and in vivo measurements of biological samples could be promoted. Overall, optimizing the imaging performances would contribute to the broader practical application of CW-THz technology in biological imaging.

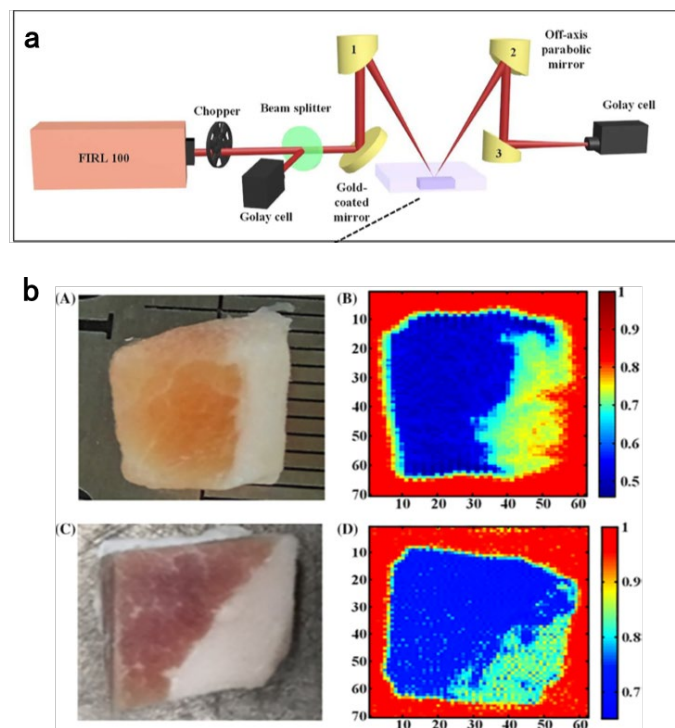


Fig. 7 (a) Experimental setup of CW-THz reflection imaging system; (b) Photos and THz images measured by p-polarized and s-polarized THz waves for pork tissues [26].

There are still some recent studies in this field. In 2018, an automatic assessment method for recognition of traumatic brain injury (TBI) based on machine learning (ML) was reported by J. Shi *et al.* using CW-THz transmission imaging [27]. In this work, a new feature extraction method for biological THz images was proposed, which combined the transmission distribution characteristics in the spatial domain and the statistical distribution characteristics in the normalized gray histogram. Based on the extracted feature database, different degrees of TBI were classified by feature selection and parameter optimization. The highest classification accuracy could reach 87.5%. In 2018, a CW-THz solid-state immersion microscopy method was developed and applied in measuring soft biological tissues by N. V. Chernomyrdin *et al.* [28]. THz images of various soft tissues were acquired, including plant leaves, cellular spheres, and in vitro breast tissue. The experimental results clearly showed sub-wavelength features of these tissues. In 2019, a CW-THz reflection imaging system was used by L. M. Wu *et al.* to inspect brain gliomas in mouse and fresh brain tissue in vitro of mouse [29]. Tumor areas in vivo and in isolated brain tissue could be well distinguished based on the intensity of THz images at 2.52 THz. THz spectral differences between brain gliomas and normal brain tissue were obtained, which presented that brain gliomas had a higher refractive index and absorption coefficient. This work suggested that CW-THz imaging had a great potential as an alternative to marker-free intraoperative diagnosis of brain gliomas in vivo. In 2019, a hybrid region of interest (ROI) segmentation method for CW-THz imaging was proposed by Y. Y. Wang *et al.* [30]. The method combined block matching 3D denoising, fuzzy c-means clustering, morphological manipulation, and smart edge detection. THz images of isolated rat brains were measured using this method. The accuracy, sensitivity, and specificity of the tumor region could separately reach 95.6%, 84.5% and 97.7%. The results showed that the hybrid ROI segmentation method performed well for CW-THz biological imaging.

#### **D. Communication and Data Transmission**

With the development of 5G and future 6G communication technology, the application of THz frequency bands has become an important development direction in communications. CW-THz has strong application prospects in high-speed communication, data transmission and wireless communication due to its ultra-high frequency, large bandwidth, and low latency properties. Comparing to traditional wireless communication technology, THz communications could meet requirements of future ultra-high-speed networks for data transmission speed and capacity. In 2024, W. P. Li *et al.* combined high-gain, high-sensitivity THz modules and signal processing technology and successfully achieved the transmission of a 50 Gbit/s net rate over 850 meters at a carrier frequency of 320 GHz [31]. The experimental arrangement for outdoor photonic THz wireless

transmission at a distance of 850 meters was shown in Fig. 8. The entire device consisted of a central station and two base stations (base station 1 and base station 2) which simulated different parts of the communication network. The function of the central station was to modulate the baseband signal. After receiving the signal transmitted by the central station through single-mode fiber 28 (SMF-28), the station 1 generated THz wireless signals through optical mixing. The function of base station 2 was to receive the THz signal and perform frequency down-conversion for future processing. At the central station, a pair of external cavity lasers (ECL1 and ECL2) with a linewidth of  $<100$  kHz transmitted continuous waves with a frequency interval of 320 GHz. The baseband signal was generated offline in the electrical domain using MATLAB/PYTHON software. Then, the signal was loaded into the arbitrary waveform generator. In the I/Q modulator, the continuous wave generated by ECL1 was modulated by the baseband signal amplified by a pair of parallel electrical amplifiers (EAs) with a gain of 25 dB. The output power of this I/Q modulator was about 0 dBm, so an erbium-doped fiber amplifier (EDFA) was used to compensate for the insertion loss of the modulator. The enhanced optical signal was combined with the 10 dBm continuous wave emitted by ECL2 through an optical coupler (OC). Then, the signal was transmitted into the base station 1 through a piece of SMF-28. In the station, an EDFA was used to amplify the power of the optical signal and change the input optical power of the UTC-PD. In this study, the photon generation of THz signals was realized using a compact rectangular waveguide coupled UTC-PD (280-380 GHz, 100 GHz bandwidth) module. The UTC-PD provided a high downlink bandwidth of 3 dB and a high saturated output power. Since the conversion efficiency of the UTC-PD was  $0.15$  A/W, considering that the output power of the UTC-PD depends on the input optical power, the THz output power range of the UTC-PD varied from -20 dBm to -8 dBm. Using the square wave detection law, a THz band radio signal of 320 GHz was generated in the UTC-PD. In base station 2, the 320 GHz THz signal received by HA2 was down-converted to a 10 GHz IF signal. To amplify the IF signal, an EA with a gain of 26 dB was used. Then, a digital storage oscilloscope (OSC) with a sampling rate of 100 GSa/s was used to capture the IF signal for offline DSP on the Rx side. Experimental results showed that single-channel THz band transmission with a net rate of 50 Gbit/s was successfully achieved over a wireless link of 850 meters with the low-emission normalized transmitter THz power of  $3.7 \times 10^{-18}$  J · bit<sup>-1</sup> · m<sup>-1</sup>. This work set a world record for the longest wireless distance and maximum distance rate product.

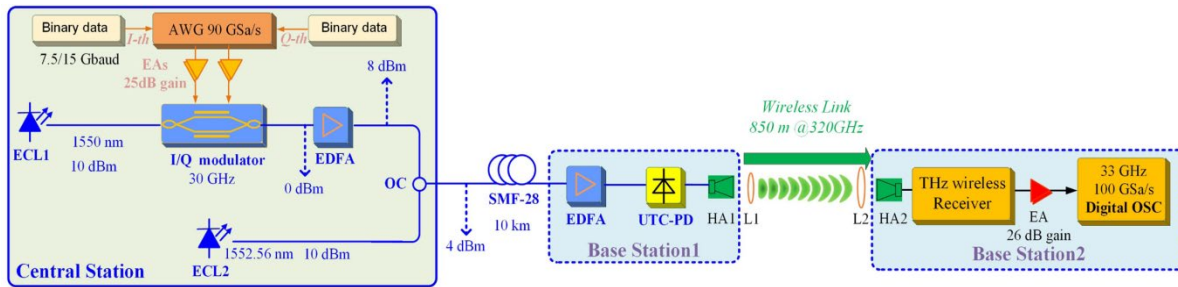


Fig. 8 Experimental setup for wireless transmission of photonic THz signals over a distance of 850 m [31].

In 2024, K. Liu *et al.* reported a 0.22 THz communication system that could provide an air interface rate of 84 Gbps over a distance of 1.26 km [32]. At the 31st International University Sports Federation held in Chengdu, China, this system was successfully applied to achieve real-time transmission of uncompressed 8K ultra-high-definition video. It made a leap forward in the THz system from experiment to promising application. The overall architecture of the system was shown in Fig. 9(a), which was mainly composed of field programmable gate array (FPGA), analog-to-digital converter (ADC), digital-to-analog converter (DAC), filter, local oscillator, IQ mixer, frequency multiplier, subharmonic mixer (SHM), duplexer, power amplifier (PA) and noise amplifier (LNA). The system could ensure 8K video transmission. The real-time video captured by the 8K camera was used as the input data source, which was operated by the camera control unit (CCU) and sent to the baseband platform through an optical fiber in the form of a high-speed data stream based on the serial digital interface (SDI) protocol. After processing the signal in the baseband module and the intermediate frequency (IF) module, the encoded and modulated signal would be transmitted by the THz Tx RF module. Then, the signal would be received by the THz Rx RF module. Finally, the video was converted to the high-definition multimedia interface (HDMI) format and displayed on the 8K TV screen after demodulation and decoding. Here, the hardware architecture integration of the THz wireless communication system was shown in Fig. 9(b). The 8K video data stream was divided into four 4K video streams, namely the upper left (LT), upper right (RT), lower left (LB) and lower right (RB). After the division, the baseband received the video data in SDI format and baseband signal processing of Tx and Rx was operated by two high-performance FPGAs. Each FPGA conducted signals of two channels consisting of 4K video streams. The dual digital-to-analog converters (DACs) generated two branches of in-phase (I) and quadrature (Q) for each 4K video stream in Tx. At the same time, each 4K video stream of Rx used a dual analog-to-digital converter (ADC) to receive the I and Q branches. At Tx, the analog signal outputted by the DAC was sent to the IQ mixer with 9 GHz as the IF LO. Then, the intermediate frequency signal in the range of 6.3 GHz-11.7 GHz was mixed into the THz frequency band through

the harmonics of the THz mixer. The THz mixer used the second harmonic generated by multiplying the frequency of the local oscillator signal for mixing. The THz local oscillator was generated by RF LO1 ~ 4 in the RF module, as shown in Fig. 9(c), where the four THz local oscillators generated are 212.8 GHz, 218.4 GHz, 207.2 GHz and 212.8 GHz respectively. The total bandwidth of the THz wireless communication system was  $5.25\text{ GHz} \times 4 = 21\text{ GHz}$ . This work focused on the practical application of the THz wireless communication system and built a real-time THz wireless communication system by integrating existing commercial components (such as FPGA and ADC/DAC), low-complexity baseband algorithms, and newly designed RF components. The results collected at FISU showed that under 16QAM-OFDM modulation, the air interface rate achieved 84 Gbps, the transmission delay was less than  $48.9048\ \mu\text{s}$ , and the bit error rate was zero within 2 hours of continuous observation, meeting the ultra-reliable requirements. In addition, the system could successfully support 8K uncompressed live video transmission at a distance of 1260 m. It was a key step in bringing THz systems from experiments to commercial applications.

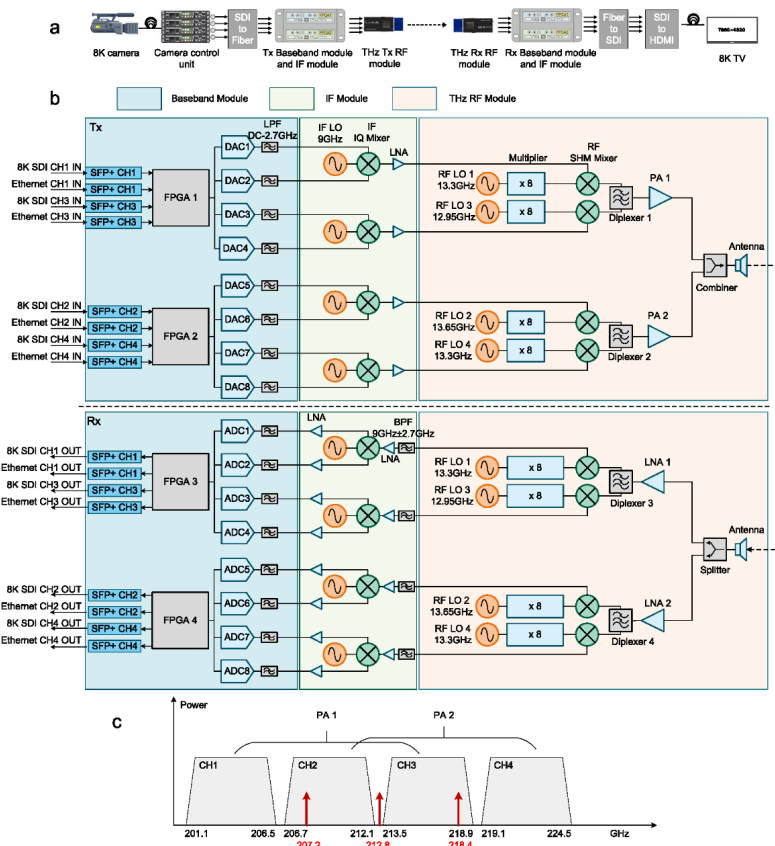


Fig. 9 Architecture and spectrum usage of THz wireless communication system. (a) Overall architecture of the system; (b) Integration of system hardware architecture; (c) THz frequency band usage. The gray part represented the frequency bands of four channels, and the red mark represents the THz local oscillator frequency [32].

In addition, there are still some recent studies in this field. In 2023, basic researches on the devices (transceivers) and systems (links) were fulfilled by M. H. Bergen *et al.* for future THz wireless communication systems [33]. The study was based on recent properties of THz emitters and detectors as well as the experimental and theoretical properties of THz reverse modulators. This work showed that passive THz transceivers with angular cones and spherical cone mirrors could work effectively on passive terahertz links and the spherical cone mirrors provided a larger angular field of view. In 2024, a frequency modulated (FM) CW-THz source was achieved by M. Miyamoto *et al.* by using Josephson junctions [34]. When a 3 GHz sine wave was superimposed on the 840-890 GHz carrier of the Josephson plasma emission (JPE), FM bandwidth of up to 40 GHz could be achieved. The results verified that the instantaneous JPE frequency followed the gigahertz modulation bias voltage. Wideband FM THz generated by a monolithic device was in stark contrast to mode-locked frequency combs built on the workbench using highly complex optics. A further increase in the modulation amplitude facilitated up-conversion or down-conversion of the frequency over multiple octaves. Compared with AM waves, the obtained FM bandwidth was two orders of magnitude higher in demodulated signal-to-noise ratio.

#### 4. Current Problems

Although CW-THz technology has shown great application potentials in many fields, several technical challenges and problems existed. These issues mainly focus on the signal attenuation, device sensitivity, cost, and scalability of technology.

##### A. Signal attenuation and propagation loss

A THz wave suffers from significant attenuation when it propagates in the air, particularly for a long propagation distance and in environments with a high humidity. Water vapor, oxygen, and other gases have large absorption coefficients to THz waves [35], which limits practical applications of THz technology. Generally, the THz signal attenuation is more serious than that of microwaves and millimeter waves. In an outdoor environment, a THz signal is rapidly attenuated due to the water vapor absorption [36]. This issue has a serious influence on the application of THz technology in wireless communications and imaging. Recent investigations proposed possible solutions by using higher gain antennas and low loss transmission media [37]. In addition, the propagation loss problem could be also alleviated by frequency selection and beam shaping techniques to a certain degree [38].

## **B. Efficiency of THz sources and detectors**

The efficiencies of THz sources and detectors still remain technical bottlenecks for applications [39]. Output powers of current THz sources are relatively lower. Although some advancements have been acquired in studies of THz sources (such as quantum cascade lasers and free electron lasers) in recent years, output powers of THz sources are still lower compared to traditional microwave and optical sources [40]. The issue limits the performance and reliability of THz equipment in practical applications. Sensitivities of current THz detectors are also not high enough. The operations of many THz detectors requires an extremely low temperature environment, which increase the complexity and cost of equipment [41]. Furthermore, current THz detectors are still inadequate for some high-precision applications. Some detectors (such as bolometers) are sensitive to a temperature change of the ambient so that a THz signal might be obscured by a thermal noise, which seriously influence the detection accuracy. The research and development of high-efficiency, low-power, and room-temperature-operating THz sources and detectors are always key issues in this field.

## **C. System cost and integration**

Too high cost of CW-THz instruments is not benefited to the application promotion. The current mainstream CW-THz sources involve complex manufacturing processes and high-purity materials, such as quantum cascade lasers, photoconductive antennas, and frequency multiplication technology. In particular, quantum cascade lasers require high-precise molecular beam epitaxy (MBE) technology, which significantly increases production cost. High-sensitivity THz detectors are also expensive and require a low-temperature working environment (such as liquid helium refrigeration), including bolometers, superconducting detectors, and so on. These problems further raise operating costs [42]. High-precision optical components, such as high-performance collimating lenses, waveguides, and reflectors, are also costly due to their raw materials (such as high-purity silicon or germanium) and processing technology. In addition, CW-THz systems always suffer from difficulties in large-scale application, system integration, and commercialization. The generation, transmission, and detection of THz waves require high-performance optical elements, which typically require extremely high processing precision. It causes application difficulties on large-scale promotion. Some THz sources (such as QCLs) and detectors required low-temperature environments, which have to be equipped with bulky cooling systems, such as liquid helium refrigerators or semiconductor refrigeration equipment. The output powers of THz sources are limited and additional power amplification and stabilization equipment

are usually necessary. The issues cause further increasing system size and complicating integration with other components. Moreover, most current THz systems are still in the research and development stage. The equipment design is primarily focused on functionality rather than optimization for portability or integration. As a result, the commercialization of CW-THz technology in the short term still remains challenging [43].

## 5. Conclusions

Because of unique properties of CW-THz technology, powerful application potentials have been demonstrated in many fields. The THz radiation is employed to non-destructively detect internal defects in non-polar materials, such as composite materials, ceramics, and semiconductors. It is very valuable in aerospace, industrial manufacturing, and electronic packaging. Based on the high transmittance of the THz radiation to packaging materials and clothes, THz security scanners could readily identify concealed dangerous items (such as explosives and weapons) without physical contacting with objects in airport and customs. CW-THz imaging could be utilized in biological sensing and chemical detection to achieve medical diagnosis and substance property characterization, which could sensitively reflect different optical responses of various substances in the THz frequency range. In addition, THz technology supports ultra-high-speed wireless communications, which could achieve ultra-high bandwidth and low-latency communications in high-frequency bands. It is a key candidate for the next generation of communication technology.

With the rapid development of CW-THz technology, its system performances would be further exploited in the future. The signal attenuation problem would be solved through the optimization of transmission media, beam shaping, and advanced modulation technologies. The sensitivities of THz detectors would be improved by developing highly sensitive and adaptable detector technologies, such as quantum detectors and superconducting detectors operating at room temperature. In concealed object detection and non-destructive testing, CW-THz technology could be integrated with robotics and automation technology to further improve inspection efficiency and accuracy. In the medical field, it is possible that CW-THz technology is combined with artificial intelligence and machine learning to fulfill more accurate disease diagnosis and personalized treatment. In addition, special filters and compensation algorithms could be developed to mitigate the attenuation effect of the ambient environment to THz waves. Recently, significant advancements of CW-THz technology have been realized in concealed object detection, non-

destructive testing, biological imaging, and other fields. In the future, it could be envisioned that CW-THz technology would be further commercialized through technological innovation, equipment optimization, and cost control. CW-THz technology would bring revolutionary changes to industry, medicine, communications, and astronomical observation.

## References

- [1] A. W. Lee and Q. Hu. “Real-time, continuous-wave terahertz imaging by use of a microbolometer focal-plane array.” *Opt. Lett.*, vol. 30, no. 19, pp. 2563–2565, Oct (2005), doi: [10.1364/OL.30.002563](https://doi.org/10.1364/OL.30.002563).
- [2] Y.-S. Lee. “Continuous-wave terahertz sources and detectors”. in *Principles of Terahertz Science and Technology*, Boston, MA: Springer US (2009), pp. 1–41. doi: [10.1007/978-0-387-09540-0\\_4](https://doi.org/10.1007/978-0-387-09540-0_4).
- [3] X. Luo, H. Zhu, T. Zhang, et al. “A 200-GHz GaN-based frequency doubler with bidirectional electro-thermal coupling method”. *IEEE Microw. Wirel. Technol. Lett.*, vol. 34, no. 7, pp. 931–934, Jul (2024), doi: [10.1109/LMWT.2024.3398001](https://doi.org/10.1109/LMWT.2024.3398001).
- [4] W. Shi and Y. J. Ding. “Continuously tunable and coherent terahertz radiation by means of phase-matched difference-frequency generation in zinc germanium phosphide”. *Appl. Phys. Lett.*, vol. 83, no. 5, pp. 848–850, Aug (2003), doi: [10.1063/1.1596730](https://doi.org/10.1063/1.1596730).
- [5] Y. J. Ding. “Progress in terahertz sources based on difference-frequency generation [invited]”. *Josa B*, vol. 31, no. 11, pp. 2696–2711, Nov. (2014), doi: [10.1364/JOSAB.31.002696](https://doi.org/10.1364/JOSAB.31.002696).
- [6] R. Köhler *et al.* “High-performance continuous-wave operation of superlattice terahertz quantum-cascade lasers”. *Appl. Phys. Lett.*, vol. 82, no. 10, pp. 1518–1520, Mar (2003), doi: [10.1063/1.1559419](https://doi.org/10.1063/1.1559419).
- [7] C. Worrall *et al.* “Continuous wave operation of a superlattice quantum cascade laser emitting at 2 THz”. *Opt. Express*, vol. 14, no. 1, pp. 171–181, Jan (2006), doi: [10.1364/OPEX.14.000171](https://doi.org/10.1364/OPEX.14.000171).
- [8] J. Li and J. Li. “Terahertz (THz) generator and detection”. *Electr. Sci. Eng.*, vol. 2, no. 1, Art. no. 1, Apr (2020), doi: [10.30564/ese.v2i1.1777](https://doi.org/10.30564/ese.v2i1.1777).
- [9] R. A. Lewis. “A review of terahertz detectors”. *J. Phys. D: Appl. Phys.*, vol. 52, no. 43, p. 433001, Aug (2019), doi: [10.1088/1361-6463/ab31d5](https://doi.org/10.1088/1361-6463/ab31d5).
- [10] E. Castro-Camus and M. Alfaro, “Photoconductive devices for terahertz pulsed spectroscopy: a review [invited],” *Photonics Res.*, vol. 4, no. 3, pp. A36–A42, Jun. 2016, doi: [10.1364/PRJ.4.000A36](https://doi.org/10.1364/PRJ.4.000A36).
- [11] H. Song, S. Hwang, H. An, et al.. “Continuous-wave THz vector imaging system utilizing two-tone signal generation and self-mixing detection”. *Opt. Express*, vol. 25, no. 17, pp. 20718–20726, Aug (2017), doi: [10.1364/OE.25.020718](https://doi.org/10.1364/OE.25.020718).
- [12] G.-J. Kim, J.-I. Kim, S.-G. Jeon, et al. “Enhanced continuous-wave terahertz imaging with a horn antenna for food inspection”. *J. Infrared, Millimeter, Terahertz Waves*, vol. 33, no. 6, pp. 657–664, Jun.(2012), doi: [10.1007/s10762-012-9902-1](https://doi.org/10.1007/s10762-012-9902-1).

- [13] Y. C. Wang, X. K. Wang, and Y. Zhang. “Reflective terahertz continuous wave linear array scanning imaging system”. *Journal of Capital Normal University (Natural Science Edition)*, vol. 45, no. 2, pp. 36–42 (2024), doi: [10.19789/j.1004-9398.2024.02.004](https://doi.org/10.19789/j.1004-9398.2024.02.004).
- [14] S.-T. Han, A. C. Torrezan, J. R. Sirigiri, et al. “Real-time, T-ray imaging using a sub-terahertz gyrotron”. *J. Korean Phys. Soc.*, vol. 60, no. 11, pp. 1857–1861, Jun (2012), doi: [10.3938/jkps.60.1857](https://doi.org/10.3938/jkps.60.1857).
- [15] S.-P. Han *et al.* “Real-time continuous-wave terahertz line scanner based on a compact 1 x 240 InGaAs schottky barrier diode array detector”. *Opt. Express*, vol. 22, no. 23, pp. 28977–28983, Nov (2014), doi: [10.1364/OE.22.028977](https://doi.org/10.1364/OE.22.028977).
- [16] J. Grzyb, K. Statnikov, N. Sarmah, et al. “A 210–270-GHz circularly polarized FMCW radar with a single-lens-coupled SiGe HBT chip”. *IEEE Trans. THz Sci. Technol.*, vol. 6, no. 6, pp. 771–783, Nov (2016), doi: [10.1109/TTHZ.2016.2602539](https://doi.org/10.1109/TTHZ.2016.2602539).
- [17] D. Wang *et al.* “Extended depth of field in continuous-wave terahertz computed tomography based on Bessel beam”. *Opt. Commun.*, vol. 432, pp. 20–26, Feb (2019), doi: [10.1016/j.optcom.2018.09.031](https://doi.org/10.1016/j.optcom.2018.09.031).
- [18] Z. -Y. Zhou, F. -S. Nian, and C. Sun. “Terahertz perspective ranging technology based on frequency modulated continuous wave”. *J. Electron. Meas. Instrum.*, vol. 37, no. 11, pp. 143–151, Jan (2024), doi: [10.13382/j.jemi.B2306843](https://doi.org/10.13382/j.jemi.B2306843).
- [19] B. Wang, X. K. Wang, Y. Yu, et al. “Terahertz Linear Array Fast Scanning Imaging”. *Chin. J. Lasers*, vol. 46, no. 6, p. 614029 (2019), doi: [10.3788/CJL201946.0614029](https://doi.org/10.3788/CJL201946.0614029).
- [20] J. Hu *et al.* “Autonomous dynamic line-scan continuous-wave terahertz non-destructive inspection system combined with unsupervised exposure fusion”. *NDT & E Int.*, vol. 132, p. 102705, Dec (2022), doi: [10.1016/j.ndteint.2022.102705](https://doi.org/10.1016/j.ndteint.2022.102705).
- [21] B. N. Kumar *et al.* “Nondestructive evaluation of cryofoam with uneven surface by continuous wave terahertz imaging using dynamic depth focusing technique”. *J. Nondestr. Eval.*, vol. 42, no. 4, p. 103, Nov (2023), doi: [10.1007/s10921-023-01015-y](https://doi.org/10.1007/s10921-023-01015-y).
- [22] Y. Zhou *et al.* “High-precision terahertz frequency modulated continuous wave imaging method using continuous wavelet transform”. *Opt. Eng.*, vol. 57, no. 2, p. 23108, Feb (2018), doi: [10.1117/1.OE.57.2.023108](https://doi.org/10.1117/1.OE.57.2.023108).
- [23] H.-S. Kim, D.-W. Park, G.-H. Oh, et al. “Non-destructive evaluation of cement hydration with pulsed and continuous terahertz electro-magnetic waves”. *Opt. Lasers Eng.*, vol. 138, p. 106414, Mar (2021), doi: [10.1016/j.optlaseng.2020.106414](https://doi.org/10.1016/j.optlaseng.2020.106414).
- [24] J. Xu, Z. Zhang, P. Yang, et al. “Nondestructive testing and 3D imaging of PE pipes using terahertz frequency-modulated continuous wave”. *Appl. Opt.*, vol. 61, no. 34, pp. 10230–10239, Dec (2022), doi: [10.1364/AO.468851](https://doi.org/10.1364/AO.468851).
- [25] B. Li, D. Wang, L. Rong, et al. “Application of continuous-wave terahertz computed tomography for the analysis of chicken bone structure”. *Opt. Eng.*, vol. 57, no. 2, p. 23105, Feb (2018), doi: [10.1117/1.OE.57.2.023105](https://doi.org/10.1117/1.OE.57.2.023105).
- [26] L. Wu *et al.* “Optimization for continuous-wave terahertz reflection imaging for biological tissues”. *J. Biophotonics*, vol. 15, no. 1, p. e202100245 (2022), doi: [10.1002/jbio.202100245](https://doi.org/10.1002/jbio.202100245).
- [27] J. Shi *et al.* “Automatic evaluation of traumatic brain injury based on terahertz imaging with machine learning”. *Opt. Express*, vol. 26, no. 5, pp. 6371–6381, Mar (2018), doi: [10.1364/OE.26.006371](https://doi.org/10.1364/OE.26.006371).
- [28] N. V. Chernomyrdin *et al.* “Reflection-mode continuous-wave 0.15 $\lambda$ -resolution terahertz solid immersion microscopy of soft biological tissues”. *Appl. Phys. Lett.*, vol. 113, no. 11, p. 111102, Sep (2018), doi: [10.1063/1.5038888](https://doi.org/10.1063/1.5038888).

10.1063/1.5045480.

- [29] L. Wu *et al.* “Study of in vivo brain glioma in a mouse model using continuous-wave terahertz reflection imaging”. *Biomed. Opt. Express*, vol. 10, no. 8, pp. 3953–3962, Aug (2019), doi: [10.1364/BOE.10.003953](https://doi.org/10.1364/BOE.10.003953).
- [30] Y. Wang *et al.* “A hybrid method based region of interest segmentation for continuous wave terahertz imaging”. *J. Phys. D: Appl. Phys.*, vol. 53, no. 9, p. 095403, Dec (2019), doi: [10.1088/1361-6463/ab58b6](https://doi.org/10.1088/1361-6463/ab58b6).
- [31] W. Li *et al.* “Photonic terahertz wireless communication: towards the goal of high-speed kilometer-level transmission”. *J. Lightwave Technol.*, vol. 42, no. 3, pp.1159–1172, Feb (2024), doi: [10.1109/JLT.2023.3329351](https://doi.org/10.1109/JLT.2023.3329351).
- [32] K. Liu *et al.* “High-speed 0.22 THz communication system with 84 Gbps for real-time uncompressed 8K video transmission of live events”. *Nat. Commun.*, vol. 15, no. 1, p. 8037, Sep (2024), doi: [10.1038/s41467-024-52370-x](https://doi.org/10.1038/s41467-024-52370-x).
- [33] M. H. Bergen, S. N. Lowry, M. E. Mitchell, et al. “Terahertz wireless communication systems: challenges and solutions for realizations of effective bidirectional links”. *Opt. Contin.*, vol. 2, no. 10, pp. 2154–2177, Oct (2023), doi: [10.1364/OPTCON.500014](https://doi.org/10.1364/OPTCON.500014).
- [34] M. Miyamoto, R. Kobayashi, G. Kuwano, et al. “Wide-band frequency modulation of a terahertz intrinsic josephson junction emitter of a cuprate superconductor”. *Nat. Photonics*, vol. 18, no. 3, pp. 267–275, Mar (2024), doi: [10.1038/s41566-023-01348-0](https://doi.org/10.1038/s41566-023-01348-0).
- [35] A. D’Arco *et al.* “Terahertz continuous wave spectroscopy: a portable advanced method for atmospheric gas sensing”. *Opt. Express*, vol. 30, no. 11, pp. 19005–19016, May (2022), doi: [10.1364/OE.456022](https://doi.org/10.1364/OE.456022).
- [36] I. F. Akyildiz, C. Han, Z. Hu, et al. “Terahertz band communication: an old problem revisited and research directions for the next decade”. *IEEE Trans. Commun.*, vol. 70, no. 6, pp. 4250–4285, Jun (2022), doi: [10.1109/TCOMM.2022.3171800](https://doi.org/10.1109/TCOMM.2022.3171800).
- [37] M. T. Nguyen, A. F. A. Hasan, and T. R. Gazizov. “Sparse wire grid UHF-band pyramidal horn antenna”. in *2024 International Russian Automation Conference (RusAutoCon)*, Sep (2024), pp. 449–455. doi: [10.1109/RusAutoCon61949.2024.10694540](https://doi.org/10.1109/RusAutoCon61949.2024.10694540).
- [38] X.-R. Zheng, D.-N. Ma, G.-T. Jiang, et al. “Terahertz shaping technology based on coherent beam combining”. *Chin. Phys. B*, vol. 32, no. 11, p. 114210, Nov (2023), doi: [10.1088/1674-1056/acc2b0](https://doi.org/10.1088/1674-1056/acc2b0).
- [39] G. Chattopadhyay. “Technology, capabilities, and performance of low power terahertz sources”. *IEEE Trans. THz Sci. Technol.*, vol. 1, no. 1, pp. 33–53, Sep (2011), doi: [10.1109/TTHZ.2011.2159561](https://doi.org/10.1109/TTHZ.2011.2159561).
- [40] S. Hayashi, K. Nawata, T. Taira, et al. “Ultrabright continuously tunable terahertz-wave generation at room temperature”. *Sci. Rep.*, vol. 4, no. 1, p. 5045, Jun (2014), doi: [10.1038/srep05045](https://doi.org/10.1038/srep05045).
- [41] Z. Z. Zhang, H. Li, and J. C. Cao. “Ultrafast terahertz detectors”. *Acta Phys. Sinica*, vol. 67, no. 9, pp. 90702–90702 (2018), doi: [10.7498/aps.67.20180226](https://doi.org/10.7498/aps.67.20180226).
- [42] A. Rogalski, M. Kopytko, and P. Martyniuk. “Two-dimensional infrared and terahertz detectors: outlook and status”. *Appl. Phys. Rev.*, vol. 6, no. 2, p. 21316, Jun (2019), doi: [10.1063/1.5088578](https://doi.org/10.1063/1.5088578).
- [43] L. Yi *et al.* “Towards practical terahertz imaging system with compact continuous wave transceiver”. *J. Lightwave Technol.*, vol. 39, no. 24, pp. 7850–7861, Dec (2021), doi: [10.1109/JLT.2021.3092779](https://doi.org/10.1109/JLT.2021.3092779).